First-principles analysis of the optical properties of structural disorder in SiO_2 glass

Tomoyuki Tamura,[1] Shoji Ishibashi,[1] Shingo Tanaka,[2] Masanori Kohyama,[2] and Ming-Hsien Lee[3]
[1]*Research Institute for Computational Sciences (RICS), National Institute of Advanced Industrial Science and Technology (AIST), Tsukuba, Ibaraki 305-8568, Japan*
[2]*Materials Science Research Group, Research Institute for Ubiquitous Energy Devices, National Institute of Advanced Industrial Science and Technology, 1-8-31, Midorigaoka, Ikeda, Osaka 563-8577, Japan*
[3]*Department of Physics, Tamkang University, Tamsui, Taipei 251, Taiwan*
(Received 25 June 2007; published 25 February 2008)

We have carried out a band-resolved analysis of the optical absorption spectra of structural disorder in SiO_2 glass by using a first-principles method, where dominant orbitals involved in the absorption spectra can be analyzed. We provided a strong theoretical support to a model where heavily strained bonds in three-membered ring structures affect the fundamental absorption edge. We found that the main absorption peak induced by an oxygen vacancy can be ascribed to a transition between the occupied and unoccupied defect states consisting of Si-Si and neighboring O orbitals due to the structural disorder. The present scheme is effective for analyzing the relationship between microscopic atomic structures and macroscopic optical properties.

DOI: 10.1103/PhysRevB.77.085207 PACS number(s): 61.43.Fs, 61.72.J−, 71.15.Mb

I. INTRODUCTION

Amorphous SiO_2 (SiO_2 glass) is one of the most important transparent materials for deep ultraviolet (duv, 200–300 nm) and vacuum ultraviolet (vuv, below 200 nm) light.[1,2] Its uv transmission limit determined by the fundamental absorption tail is located at 8–9 eV, which is the largest among the known amorphous oxides. Despite the low metallic impurity content in industrial products, the transmittance of synthetic SiO_2 glasses in the duv-vuv spectral region is often far from the theoretical limit determined by the fundamental absorption edge and the Rayleigh scattering. The main origin of the discrepancy lies in the structural defects formed in the manufacturing process or induced by exposure to the duv-vuv light.[3] The existence of these defects is very harmful for several industrial applications of SiO_2 glass. In optical fibers, the transmission loss due to the structural defects is significantly magnified because of the large optical path length. Thus, control of the structural defects in SiO_2 glasses is a key issue in developing optical fibers for use in the duv-vuv region.

Extensive experimental and theoretical studies have been devoted to structural defects in SiO_2 glass, and these defects can be classified into two categories.[4] The first is a defect defined as chemical disorder such as oxygen-deficient centers (ODCs) and E' centers,[5–8] and the second is defined as physical disorder such as bond-angle deviations and various kinds of $(Si-O)_n$ ring structures.[9] Closed paths containing n Si-O bonds are referred to as n-membered rings, in contrast to the usual six- and eight-membered rings in crystalline quartz. Identification or characterization of the structural defects is made by various spectroscopic techniques such as optical absorption (OA) and photoluminescence (PL) spectra, and electron paramagnetic resonance (EPR) for paramagnetic defects. Among structural defects in SiO_2 glass, ODCs have been highlighted in several recent reviews.[1] There is a widely shared opinion that an optical absorption band with a maximum around 7.6 eV in SiO_2 glass can be ascribed to Si ODCs,[8] but this assignment is still being questioned.[10] On the other hand, Raman and optical spectroscopy measurements combined with EPR give us information about the relationship between the optical properties and the structural disorder. Several observations have suggested that the vuv transparency of SiO_2 glass depends on the Si-O-Si angle. In densified SiO_2 glass, the average Si-O-Si angle decreases[11] and the fundamental absorption edge shifts to the lower-energy side.[12] The band gap of SiO_2 glass, which is smaller than that of crystalline α-quartz,[13] seems to be dominated by such structural disorder or defects. It is important to control the degree of disorder or densities of defects in SiO_2 glass to improve the transparency. But the origin of the fundamental absorption edge itself is still controversial. Thus we have to clarify the effects of the structural disorder or defects on the optical properties.

On the theoretical side, supercell band calculations based on density functional theory (DFT) have contributed to the understanding of the optical properties of solid materials through the sum-over-states formalism in spite of the limitations of the DFT. However, it is not so easy to clarify the relationship between the local structural features and the optical properties by such supercell calculations. In order to investigate the optical transition mechanism, Lee and co-workers proposed a so-called band-resolved analysis technique.[14,15] Using this technique, the local contribution to the optical properties involved in the transitions at specific photon energies can be directly clarified within the band theory.

In this paper, in order to understand the microscopic origins of the fundamental optical properties of vuv-transparent SiO_2 glass, first, we perform a band-resolved analysis of the absorption spectra of SiO_2 glass with the usual continuous-network configuration. We analyze the main contribution to the fundamental absorption edge. Second, we examine the effects of a Si ODC on the absorption spectrum of SiO_2 glass, where defect-induced absorption peaks are analyzed. We deal with a neutral Si-Si dimer model as one possible model of the Si ODC.

II. METHOD

The present calculations on SiO_2 glass were performed by using our original computational code QMAS (Quantum MAterials Simulator).[16] We adopted the projector augmented-wave (PAW) method[17–19] with the generalized gradient approximation[20] (GGA) for the electronic exchange and correlation interactions. We dealt with a periodic cubic cell of nondefected amorphous SiO_2 (a-SiO_2) with the size of 11.32 Å and containing 32 Si and 64 O atoms. In Ref. 21, an undefected model configuration at the experimental density of 2.20 g/cm^3 was generated by quenching, using a classical molecular dynamics method and subsequent relaxation using the first-principles norm-conserving pseudopotential (NCPP) method[22,23] within the local density approximation (LDA).[24] We performed additional atomic relaxation of this configuration, keeping the cell size fixed, by using the present PAW-GGA scheme. It should be noted that the PAW-GGA scheme is more accurate than the NCPP-LDA scheme due to the higher transferability of the PAW potentials for various local environments. Also, for the optical properties, the PAW-GGA scheme is more robust because it includes the accurate radial behavior of wave functions near the nuclei. The plane-wave cutoff energy of 35 Ry was used. Of the k points, only the Γ point was used because of the large size of the supercell modeling an amorphous structure. We have confirmed that the present results are consistent with those obtained by using a $2\times2\times2$ k-point mesh. We also performed first-principles calculations of crystalline α-quartz (q-SiO_2) for comparison, with the same computational conditions, where one special k point per irreducible part of the Brillouin zone for structural optimization and an $8\times8\times8$ mesh for the optical properties were used. In order to calculate optical properties, it is desirable to include a large number of unoccupied bands, and we adopted twice the total number of valence bands throughout this work. For crystalline α-quartz, we have confirmed that the top of the unoccupied bands is located at about 30 eV above the top of the valence band, and that the calculation of the dielectric constant is well converged (see Table II later).

The complex dielectric function $\epsilon(\omega)=\epsilon_1(\omega)+i\epsilon_2(\omega)$ is known to describe the linear optical response of the medium at all photon energies, e.g., the refractive index n, the extinction coefficient k, and the absorption coefficient α. These optical properties are calculated based on the independent-particle approximation, i.e., the excitonic effects and the local-field corrections are neglected. In order to obtain more accurate optical properties, we have to apply the GW method[25] or time-dependent density functional theory.[26,27] However, it is not possible to apply such schemes to large cells. The imaginary part of the dielectric function can be calculated using the momentum matrix elements that describe the electronic transition between the valence and conduction bands in the crystal. The formula is given by

$$\epsilon_2(\omega)=\frac{4\pi^2}{\Omega\omega^2}\sum_{\mathrm{VB,CB,k}} w_{\mathbf{k}}|p_{\mathbf{k}}^{\mathrm{VB,CB}}|^2\delta(E_{\mathbf{k}}^{\mathrm{CB}}-E_{\mathbf{k}}^{\mathrm{VB}}-\hbar\omega), \quad (1)$$

where VB and CB label valence-band and conduction-band states of the energies $E_{\mathbf{k}}^{\mathrm{VB}}$ and $E_{\mathbf{k}}^{\mathrm{CB}}$ for each k point, respectively, $w_{\mathbf{k}}$ is the kth point weighting, Ω is the crystal volume, and p are the momentum matrix elements from the self-consistent band structure within the PAW formalism. The real part of the dielectric function can be extracted from the imaginary part using the Kramers-Kronig relation:

$$\epsilon_1(\omega)=1+\frac{2}{\pi}\mathrm{P}\int_0^\infty \frac{\omega'\epsilon_2(\omega')d\omega'}{\omega'^2-\omega^2} \quad (2)$$

where P is the principal value of the integral.

Here we give a brief summary of our band-resolved analysis scheme.[14] The absorption coefficient α can be calculated as

$$\alpha(\omega)=A\sum_{\mathrm{VB,CB,k}} w_{\mathbf{k}}|p_{\mathbf{k}}^{\mathrm{VB,CB}}|^2\delta(E_{\mathbf{k}}^{\mathrm{CB}}-E_{\mathbf{k}}^{\mathrm{VB}}-\hbar\omega), \quad (3)$$

where $A=4\pi/\Omega\omega n(\omega)c$. The refractive index $n(\omega)$ in the denominator is evaluated from ϵ_1 and ϵ_2. This is decomposed into two types of representation of orbital contributions for valence and conduction bands, respectively, by changing the summing sequences as

$$\begin{aligned}\alpha^{\mathrm{VB}}(\omega,E)&=A\sum_{\mathrm{VB,k}}\left(\sum_{\mathrm{CB}} w_{\mathbf{k}}|p_{\mathbf{k}}^{\mathrm{VB,CB}}|^2\delta(E_{\mathbf{k}}^{\mathrm{CB}}-E_{\mathbf{k}}^{\mathrm{VB}}-\hbar\omega)\right)\\&\quad\times\delta(E-E_{\mathbf{k}}^{\mathrm{VB}})\\&=\sum_{\mathrm{VB,k}}\alpha_{\mathbf{k}}^{\mathrm{VB}}(\omega)\delta(E-E_{\mathbf{k}}^{\mathrm{VB}})\end{aligned} \quad (4)$$

and

$$\begin{aligned}\alpha^{\mathrm{CB}}(\omega,E)&=A\sum_{\mathrm{CB,k}}\left(\sum_{\mathrm{VB}} w_{\mathbf{k}}|p_{\mathbf{k}}^{\mathrm{VB,CB}}|^2\delta(E_{\mathbf{k}}^{\mathrm{CB}}-E_{\mathbf{k}}^{\mathrm{VB}}-\hbar\omega)\right)\\&\quad\times\delta(E-E_{\mathbf{k}}^{\mathrm{CB}})\\&=\sum_{\mathrm{CB,k}}\alpha_{\mathbf{k}}^{\mathrm{CB}}(\omega)\delta(E-E_{\mathbf{k}}^{\mathrm{CB}}).\end{aligned} \quad (5)$$

We call the band-by-band decomposed absorption coefficients $\alpha_{\mathbf{k}}^{\mathrm{VB}}$ and $\alpha_{\mathbf{k}}^{\mathrm{CB}}$ the "band-resolved" partial absorption coefficients. By using the terms

$$\beta_{\mathbf{k}}^{\mathrm{VB}}(\omega)=\frac{\alpha_{\mathbf{k}}^{\mathrm{VB}}(\omega)}{\alpha(\omega)} \quad (6)$$

and

$$\beta_{\mathbf{k}}^{\mathrm{CB}}(\omega)=\frac{\alpha_{\mathbf{k}}^{\mathrm{CB}}(\omega)}{\alpha(\omega)} \quad (7)$$

in Eqs. (4) and (5), the normalized band-resolved partial absorption is obtained. Finally the distribution of partial absorption for each electronic level can be plotted through the δ functions $\delta(E-E_{\mathbf{k}}^{\mathrm{VB}})$ and $\delta(E-E_{\mathbf{k}}^{\mathrm{CB}})$. This can clarify the orbital contribution to the electronic transition at a specific photon energy in terms of the peak height.

Here it should be noted that the δ function of $\delta(E_{\mathbf{k}}^{\mathrm{CB}}-E_{\mathbf{k}}^{\mathrm{VB}}-\hbar\omega)$ is replaced by a Gaussian of 0.1 eV in practical computations of Eqs. (3)–(5) to prevent artificial effects of the supercell, namely, the discrete energy distribution of eigenstates. This scheme can also be regarded as the accumulation of the absorption processes for the photon energies

with a Gaussian distribution and a center $\hbar\omega$.

However, this point does not affect the physical features if the supercell size is sufficiently large.

We also perform so-called real-space partial electron density analysis of absorption.[15] In the PAW method, the all-electron wave function $\Psi_{\mathbf{k}}^{b}$ is derived from the pseudo-wave-function $\tilde{\Psi}_{\mathbf{k}}^{b}$ by means of a linear transformation[17–19]

$$|\Psi_{\mathbf{k}}^{b}\rangle = |\tilde{\Psi}_{\mathbf{k}}^{b}\rangle + \sum_{i} (|\phi_i\rangle - |\tilde{\phi}_i\rangle)\langle\tilde{p}_i|\tilde{\Psi}_{\mathbf{k}}^{b}\rangle. \tag{8}$$

The index i is a shorthand for the atomic site R, the angular momentum numbers $L=l,m$, and an additional index referring to the reference energy. The all-electron partial waves ϕ_i, the pseudo-partial-waves $\tilde{\phi}_i$, and the projector functions $\tilde{p}_i$ are obtained for a reference atom. The real-space partial electron density of absorption at the photon energy of $\hbar\omega$ can be evaluated using the partial contribution $\beta_{\mathbf{k}}^{b}$ in a similar way to evaluation of the all-electron total charge density (for details we refer to Refs. 17–19),

$$\alpha_{\mathbf{k}}^{\mathrm{VB}}(\omega,\vec{r}) = \sum_{\mathrm{VB}}\sum_{\mathbf{k}} \beta_{\mathbf{k}}^{\mathrm{VB}}(\omega) \times\left(|\tilde{\Psi}_{\mathbf{k}}^{\mathrm{VB}}(\vec{r})|^2 + \sum_{(i,j)} \rho_{\mathbf{k}}^{\mathrm{VB},(i,j)}(\phi_i^*\phi_j - \tilde{\phi}_i^*\tilde{\phi}_j)\right) \tag{9}$$

and

$$\alpha_{\mathbf{k}}^{\mathrm{CB}}(\omega,\vec{r}) = \sum_{\mathrm{CB}}\sum_{\mathbf{k}} \beta_{\mathbf{k}}^{\mathrm{CB}}(\omega) \times\left(|\tilde{\Psi}_{\mathbf{k}}^{\mathrm{CB}}(\vec{r})|^2 + \sum_{(i,j)} \rho_{\mathbf{k}}^{\mathrm{CB},(i,j)}(\phi_i^*\phi_j - \tilde{\phi}_i^*\tilde{\phi}_j)\right), \tag{10}$$

where

$$\rho_{\mathbf{k}}^{b,(i,j)} = \langle\tilde{\Psi}_{\mathbf{k}}^{b}(\vec{r})|\tilde{p}_i\rangle\langle\tilde{p}_j|\tilde{\Psi}_{\mathbf{k}}^{b}(\vec{r})\rangle. \tag{11}$$

For a given energy or frequency in absorption spectra, one can obtain the three-dimensional density distributions of wave functions of the occupied and unoccupied states directly involved in the optical absorption process. These should provide great insight into the relation between the local configuration and the optical properties.

III. RESULTS AND DISCUSSION

A. Undefected supercell

The short-range structural parameters of the a-SiO_2 configuration obtained by the PAW-GGA scheme are listed in Table I, as compared with those by the NCPP-LDA scheme.[21] The differences are rather small. The switching to the PAW-GGA scheme results in a slight increase of the averaged Si-O bond length. This does not induce any serious problem for the fixed cell size, because of the absorption by the rotation of SiO_4 tetrahedral units. Figure 1 shows the density of states (DOS) of a-SiO_2 as compared with q-SiO_2. The features are very similar to our previous results.[21] The

TABLE I. Short-range structural parameters for a-SiO_2. Averaged values are listed.

	Bond length (Å)	Bond angle (deg)	
	Si-O	O-Si-O	Si-O-Si
NCPP-LDA (Ref. 21)	1.616	109.48	144.97
PAW-GGA	1.625	109.48	143.03

lowest band from −19 to −17 eV is the O 2s band, the middle band from −10 to −4 eV is the O 2p and Si sp^3 hybrid bonding band, and the highest band from −3 to 0 eV is the O 2p nonbonding band. The DOS of a-SiO_2 has a similarity to that of q-SiO_2 because of the similar short-range order. However, there are substantial differences. In a-SiO_2, the peaks at the lower part of the Si-O bonding band and the peak at the bottom of the O 2p nonbonding band are smeared out. As for the conduction band, the DOS from 10 to 15 eV of a-SiO_2 has a broad band structure, but that of q-SiO_2 has well-separated peaks. The most significant difference is the shape of the conduction-band edge. The changes of the DOS from q-SiO_2 to a-SiO_2 are consistent with other first-principles results,[28,29] and in good agreement with the observed changes in the x-ray photoelectron spectroscopy (XPS) spectra.[30]

The electronic properties of a-SiO_2 and q-SiO_2 are summarized in Table II. The band gap values of q-SiO_2 and a-SiO_2 obtained from the Kohn-Sham eigenvalues are smaller than the experimental values because of the shortcomings of the DFT. We obtained a reduction of the gap value from the crystalline to amorphous phase as 0.33 eV, which is a little smaller than the experimental one of about 0.5 eV.[31] The dielectric constant ϵ_1 at 0 eV for q-SiO_2 is 2.51, which is slightly larger than the experimental value. This is caused by the underestimated energy gap. The dielectric constant of a-SiO_2 is smaller than that of q-SiO_2. This reduction from the crystalline to the amorphous phase is consistent with the experimental reduction from 2.40 to 2.10.[32]

Figure 2 shows the calculated optical absorption spectra. The calculated absorption energy gaps are smaller than the

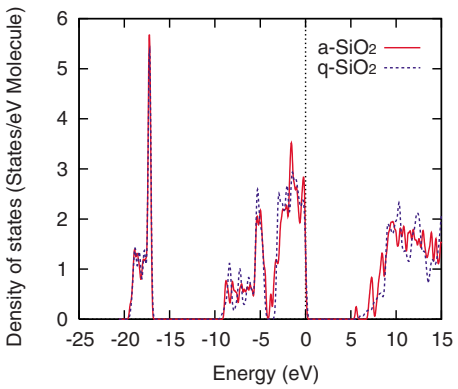

FIG. 1. (Color online) Density of states of the a-SiO_2 system as compared with q-SiO_2. The top of the valence band is chosen as 0 eV. Electronic levels are broadened with a Gaussian half-width of 0.1 eV.

TABLE II. The band gap and the dielectric constant ϵ_1 at 0 eV for q-SiO_2 and a-SiO_2. Experimental results are taken from Refs. 31 and 32.

		Band gap (eV)	Dielectric constant
q-SiO_2	This work	5.92	2.51
	Expt.	8.7–9.4	2.40
a-SiO_2	This work	5.59	2.28
	Expt.	8.4–9.0	2.10

experimental ones due to the underestimation of energy gaps obtained from the Kohn-Sham eigenvalues. The absorption of a-SiO_2 at 5.59 eV, which is the energy gap obtained from the Kohn-Sham eigenvalues, is very small. If we define the fundamental absorption edge as the photon energy at the absorption value of 100 cm^{-1}, the absorption edge is 6.35 eV for the present a-SiO_2 model and 7.00 eV for q-SiO_2. This reduction from q-SiO_2 to a-SiO_2 is a little larger than the experimental one of 0.5 eV.[31]

The fundamental absorption edge is larger than the energy gap obtained from the Kohn-Sham eigenvalues. This means that the transition from the valence-band maximum (VBM) to the conduction-band minimum (CBM) does not occur. Figure 3 shows the partial electron densities of the VBM and CBM states. As mentioned above, the highest valence band is the O $2p$ nonbonding band. The electron density of the VBM is located on oxygen atoms with p-like shapes. The electron density of the CBM is also located on oxygen atoms with s-like shapes. We cannot find apparent localization of the electron density to specific local atomic groups. The distribution on oxygen atoms is quite different between the VBM and the CBM, and thus there should be negligible transition from the VBM to the CBM. This point is also supported by our computation of the transition matrix between the VBM and CBM states. The square of the matrix element is 0.000 as compared with 0.010 for the absorption at $\hbar\omega$=7.3 eV (from the state of −1.76 eV to the CBM).

In order to analyze the origin of the fundamental absorption edge in a-SiO_2, we carried out a band-resolved analysis of the absorption spectrum at 6.35 eV using Eqs. (4)–(7) as

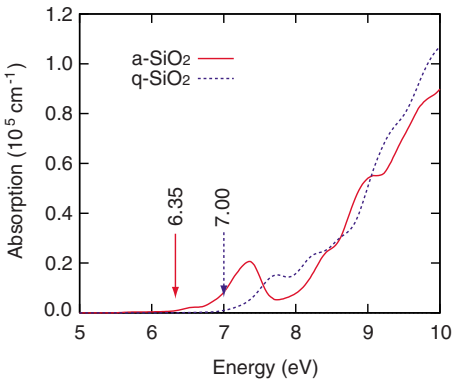

FIG. 2. (Color online) Absorption spectrum of the a-SiO_2 system as compared with q-SiO_2. The arrows indicate the calculated absorption edges.

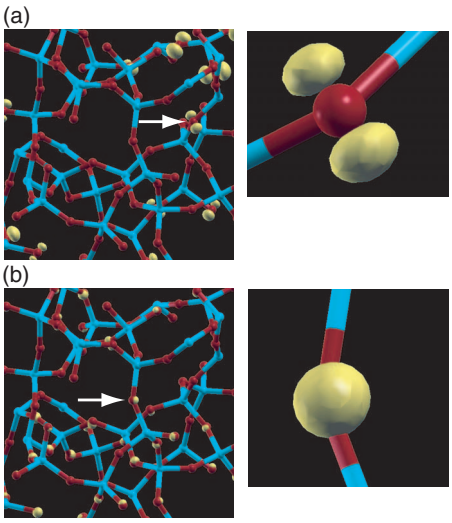

FIG. 3. (Color) Real-space partial electron densities of (a) the valence-band maximum and (b) the conduction-band minimum. The isosurfaces are plotted at 0.006 electrons/a.u.^{3} for the valence band and at 0.002 electrons/a.u.^{3} for the conduction band. Enlarged figures around oxygen atoms indicated by arrows are also shown.

shown in Fig. 4. For the valence band, peaks are distributed from −1.0 to −0.6 eV and the highest peak is located at −0.84 eV. For the conduction band, only one peak can be seen at 5.59 eV, which is the CBM state. The energy difference between the highest peak in the valence band and that in the conduction band is 6.43 eV, and the main contribution to the absorption edge is the transition between these two states.

Figure 5 shows the real-space partial electron densities of the states involved in the absorption at 6.35 eV for a-SiO_2,

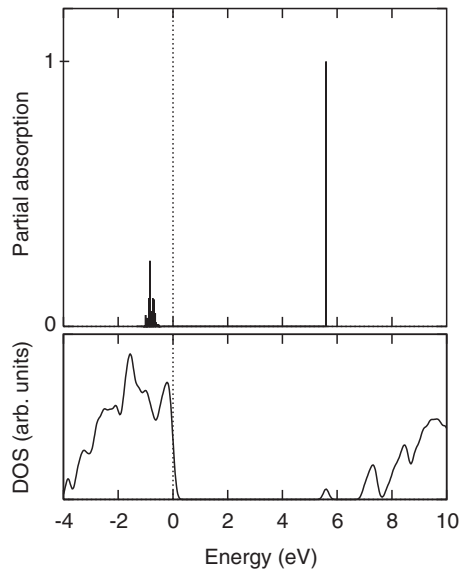

FIG. 4. Density of states of a-SiO_2 and the band-resolved partial absorption at $\hbar\omega$=6.35 eV for the valence and conduction bands. The top of the valence band is aligned at 0 eV. The decomposed partial absorption is normalized by the total absorption.

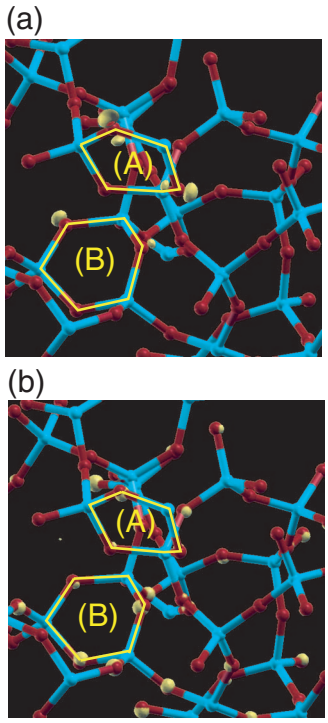

FIG. 5. (Color) Real-space partial electron densities that contribute to the absorption for a-SiO_2 at the energy of 6.35 eV for (a) the valence and (b) the conduction bands. Yellow lines indicate the three-membered rings. The isosurfaces are plotted at 0.006 electrons/a.u.^{3} for the valence band and at 0.002 electrons/a.u.^{3} for the conduction band.

obtained by Eqs. (9) and (10). For the valence band, the electron density is greatly enhanced on oxygen atoms constituting three-membered rings, although this feature could not be seen in Fig. 3(a) for the VBM. The three-membered rings (A) and (B) in Fig. 5 contain three Si-O-Si bond angles of 118.4°, 121.9°, and 133.5°, and of 124.8°, 125.2°, and 127.5°, respectively. These bond-angle values are much smaller than the averaged value 143.0° in Table I. Pasquarello *et al.* obtained similar results on the small rings, where the averaged Si-O-Si bond angle in the three-membered rings is 128.4° and is smaller than the averages over the whole sample.[33] As for the conduction band, the electron density is also located on oxygen atoms constituting three-membered rings, although the feature of localization is rather weak. Figures 3(b) and 5(b) are basically the same and only the direction of the eyes is different. These features of localization come mainly from the wave function of the electronic states that have the highest peak in the valence and the conduction bands in Fig. 4.

Two sharp lines marked by D_1=495 cm^{-1} and D_2 =606 cm^{-1} can be observed in SiO_2 glass with Raman spectroscopy, resulting from symmetric breathing modes of four-membered (D_1) and three-membered (D_2) ring structures.[34,33] The Si-O-Si bond angles in these small rings are heavily strained. Fluorine doping into dry SiO_2 glasses effectively enhances transmittance at 7.9 eV by narrowing the Si-O-Si distribution.[35] Thus it may be considered that the vuv absorption edge of SiO_2 glass is seriously affected by the concentration of strained Si-O-Si bond angles associated with such small rings. Our amorphous model contains two three-membered and two four-membered rings in the supercell, and the averaged value of Si-O-Si bond angles in the four-membered rings is 138.8°, which is much larger than that in the three-membered rings. The valence wave functions involved in the fundamental absorption edge are mainly localized in the three-membered rings as shown in Fig. 5. The present results indicate that the transition from the 2p nonbonding states of oxygen atoms in heavily strained three-membered rings contributes to the fundamental absorption edge.

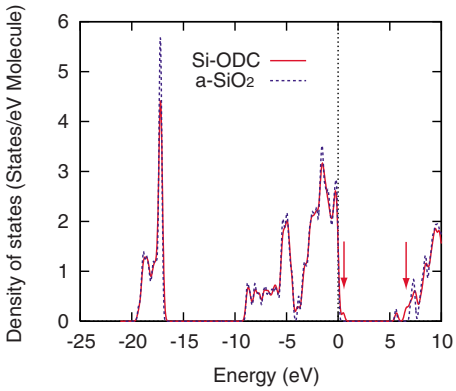

FIG. 6. (Color online) Density of states of the Si ODC system as compared with the undefected a-SiO_2. The top of the valence band of undefected a-SiO_2 is chosen as 0 eV. The arrows indicate the occupied and unoccupied defect states of the Si ODC (Si-Si dimer) system. Electronic levels are broadened with a Gaussian half-width of 0.1 eV.

B. Oxygen-deficient centers

In order to form an oxygen vacancy, we removed one oxygen atom from a Si-O-Si network in the present a-SiO_2 supercell as in our previous paper.[21] In the relaxed atomic configuration at the Si ODC, the reconstructed Si-Si bond length is 2.382 Å, which is very similar to 2.427 Å obtained by the NCPP-LDA scheme.[21] The surrounding six Si-O bonds are stretched by inducing the ODC, where the averaged bond length is changed from 1.625 to 1.651 Å. The features of the local configuration of the Si-ODC are in good agreement with previous first-principles calculations using cluster models[36–41] and periodic cells.[42–45] They show that the removal of an oxygen atom from the lattice leads to the formation of a Si-Si bond with the length of ~2.5 Å.[36]

In the DOS of the Si ODC system shown in Fig. 6, there are remarkable increases at the VBM and near the CBM as indicated by arrows. These changes are caused by the generation of one occupied and one unoccupied defect states accompanied by the removal of bulklike Si-O states and O 2p nonbonding states. The occupied state of the Si ODC exists at 0.49 eV above the bulk VBM of the undefected system, which is similar to 0.56 eV obtained by the NCPP-LDA scheme.[21] The increase in the DOS near the CBM has a peak around 6.7 eV. Note that the CBM is located at 5.65 eV,

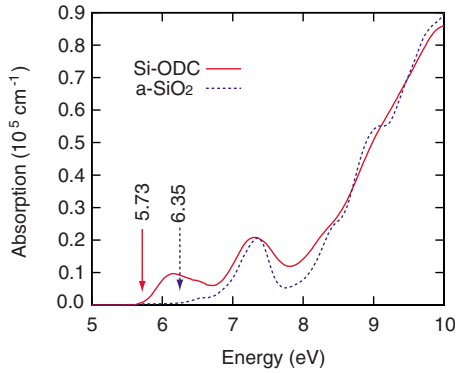

FIG. 7. (Color online) Absorption spectrum of the Si ODC system as compared with the undefected a-SiO_2. The arrows indicate the calculated absorption edge.

namely, 5.16 eV above the occupied defect level.

Figure 7 shows the calculated optical absorption spectra of the a-SiO_2 systems with and without the Si ODC. We can see the remarkable changes of the absorption in a wide energy range from 5.7 to 8.6 eV, where the absorption spectrum of the Si ODC system has a peak with a maximum at 6.15 eV. If we define the fundamental absorption edge as the photon energy at the absorption value of 100 cm^{-1}, the absorption edge for the present Si ODC system is 5.73 eV, in contrast to 5.16 eV obtained as the minimum Kohn-Sham gap and to 6.35 eV of the undefected structure. In order to analyze the contributions to the changes in the absorption spectrum, we carried out a band-resolved analysis at the energies of 5.73 and 6.15 eV.

Figure 8 shows the band-resolved partial absorption of the Si ODC system at 5.73 and 6.15 eV for the valence and conduction bands. In the case of 5.73 eV (the absorption

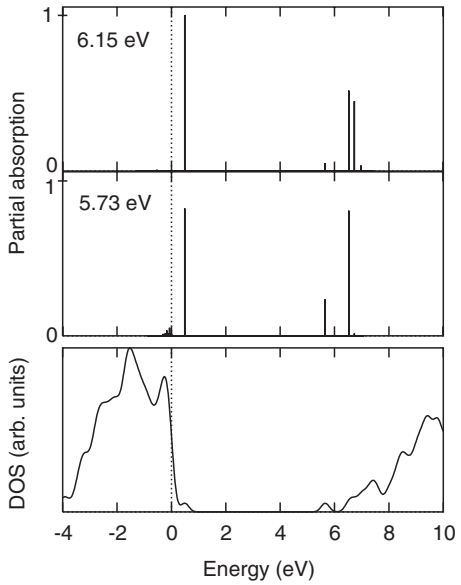

FIG. 8. Density of states of the Si ODC system and the band-resolved partial absorption at $\hbar\omega$=5.73 and 6.15 eV for the valence and conduction bands. The decomposed absorption is normalized by the total absorption.

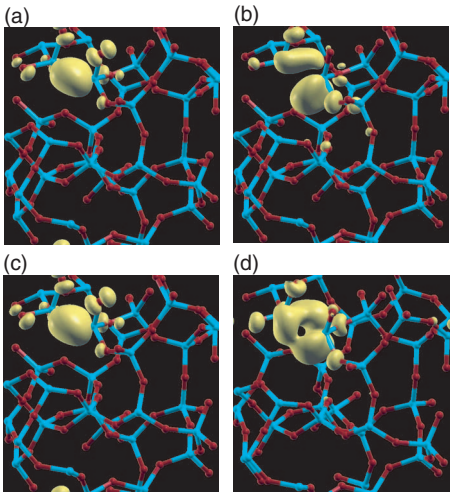

FIG. 9. (Color) Real-space partial electron densities that contribute to the absorption of the Si ODC system at 5.73 eV for (a) the valence and (b) the conduction band and at 6.15 eV for (c) the valence and (d) the conduction band. The isosurfaces are plotted at 0.004 electrons/a.u.^{3} for the valence band and 0.002 electrons/a.u.^{3} for the conduction band.

edge), the highest peaks are located at 0.49 eV for the valence band and 6.7 eV for the conduction band. In the case of 6.15 eV (the maximum of the increased absorption), the highest peaks are located at 0.49 and around 6.7 eV. It is clear that the transitions occur from the occupied defect state for both cases.

We now consider the real-space partial electron densities of the states involved in the absorption at 5.73 eV shown in Figs. 9(a) and 9(b). The electron density for the valence band is strongly localized at the Si ODC, i.e., the Si-Si bond and neighboring O atoms. This corresponds to the occupied defect state consisting of a Si-Si bonding orbital and hybridization with surrounding O 2p orbitals. In Fig. 9(b), the partial electron density for the conduction band is also located at the Si-Si bond and O atoms. However, the electron density is rather extended to neighboring atoms.

Figures 9(c) and 9(d) show the real-space partial electron densities involved in the absorption at 6.15 eV. For the valence band, the electron density corresponds to the occupied defect state, similar to the case of Fig. 9(a). The electron density for the conduction band in Fig. 9(d) clearly corresponds to the unoccupied defect state around 6.7 eV shown in Fig. 6. The density distribution on the neighboring O atoms has an s-like shape and that at the Si-Si bond has features of antibonding orbitals. It is interesting that this unoccupied defect state with rather localized features exists inside the band.

In this way, the absorption edge of the Si ODC system at 5.73 eV, which is about 0.6 eV lower than that of the undefected a-SiO_2, is dominated by the transition from the occupied defect state to a rather extended state around the defect. The maximum peak of the increased absorption at 6.15 eV is dominated by the transition from the occupied defect state to the unoccupied defect state.

From a large number of theoretical calculations based on cluster models,[36,46] it was widely believed that an optical

absorption at around 7.6 eV corresponds to the transition between the Si-Si bonding σ and antibonding σ^* states. Our present results indicate that the Si ODC indeed generates a new absorption peak below the fundamental absorption edge of a-SiO_2, through the transition between the occupied and unoccupied defect states. However, these defect states are not simply described by Si-Si bonding or antibonding orbitals, but with substantial hybridization with neighboring O orbitals due to structural disorder.

In the present work, our aim is to apply our scheme of optical-property analysis of the local configuration to one probable configuration of the oxygen vacancy. Note that the present configuration is consistent with other theoretical results. Of course, the defects in amorphous materials exhibit a very rich structure because of the large variation in local bonding,[45] and it is desirable to analyze the statistical probability in order to understand the whole nature of the oxygen vacancy. Furthermore, there exist many kinds of oxygen-deficiency-related defects.[8] The examination of such various defect configurations is beyond the scope of the present paper. We believe that our band-resolved scheme may be useful for the understanding of the optical properties of such defects.

IV. CONCLUSION

We analyzed pairs of valence-band and conduction-band states that contribute to the optical absorption using a band-resolved scheme in order to understand the effects of the structural disorder on the optical properties. We found that the partial electron density that contributes to the absorption edge in our amorphous SiO_2 model is localized on some oxygen atoms with heavily strained Si-O-Si bond angles constituting three-membered rings, and that the nature of a new absorption peak induced by an oxygen-deficient center (Si ODC) can be ascribed to a transition not simply between Si-Si bonding and antibonding states, but between realistic defect states consisting of Si-Si and neighboring O orbitals due to the structural disorder.

ACKNOWLEDGMENTS

The authors would like to thank K. Terakura for his cooperation in developing the QMAS code and for encouragement. This work was supported by the Next Generation Super Computing Project, Nanoscience Program, MEXT, Japan. M.-H.L. wishes to thank NSC (Grant No. 96-2112-M-032-004-), NCHC, and NCTS for resource support.

[1] *Defects in SiO_2 and Related Dielectrics: Science and Technology*, edited by G. Pacchioni, L. Skuja, and D. L. Griscom, NATO Science Series (Kluwer, Dordrecht, 2000).
[2] *Structure and Imperfections in Amorphous and Crystalline Silicon Dioxide*, edited by R. A. B. Devine, J-P. Duraud, and E. Dooryheé (Wiley, Chichester, U.K., 2000).
[3] L. Skuja, H. Hosono, M. Hirano, and K. Kajihara, Proc. SPIE **5112**, 2 (2003).
[4] H. Hosono, Y. Ikuta, T. Kinoshita, K. Kajihara, and M. Hirano, Phys. Rev. Lett. **87**, 175501 (2001).
[5] D. L. Griscom, in *Defects in SiO_2 and Related Dielectrics: Science and Technology* (Ref. 1), pp. 117–160.
[6] S. Agnello, R. Boscaino, F. M. Gelardi, and B. Boizot, J. Appl. Phys. **89**, 6002 (2001).
[7] S. Agnello, R. Boscaino, G. Buscarino, M. Cannas, and F. M. Gelardi, Phys. Rev. B **66**, 113201 (2002).
[8] L. Skuja, J. Non-Cryst. Solids **239**, 16 (1998).
[9] K. Awazu and H. Kawazoe, J. Appl. Phys. **94**, 6243 (2003).
[10] A. N. Trukhin and H.-J. Fitting, J. Non-Cryst. Solids **248**, 49 (1999).
[11] F. L. Galeener, J. Non-Cryst. Solids **49**, 53 (1982).
[12] R. A. B. Devine, R. Dupree, I. Farnan, and J. J. Capponi, Phys. Rev. B **35**, 2560 (1987).
[13] N. Kitamura, K. Fukumi, K. Kadono, H. Yamashita, and K. Suito, Phys. Rev. B **50**, 132 (1994).
[14] M.-H. Lee, C.-H. Yang, and J.-H. Jan, Phys. Rev. B **70**, 235110 (2004).
[15] C.-W. Chen, M.-H. Lee, and Y.-T. Lin, Appl. Phys. Lett. **89**, 223105 (2006).
[16] S. Ishibashi, T. Tamura, S. Tanaka, M. Kohyama, and K. Terakura (unpublished).
[17] P. E. Blöchl, Phys. Rev. B **50**, 17953 (1994).
[18] N. A. W. Holzwarth, G. E. Matthews, R. B. Dunning, A. R. Tackett, and Y. Zeng, Phys. Rev. B **55**, 2005 (1997).
[19] G. Kresse and D. Joubert, Phys. Rev. B **59**, 1758 (1999).
[20] J. P. Perdew, K. Burke, and M. Ernzerhof, Phys. Rev. Lett. **77**, 3865 (1996).
[21] T. Tamura, G.-H. Lu, R. Yamamoto, and M. Kohyama, Phys. Rev. B **69**, 195204 (2004).
[22] N. Troullier and J. L. Martins, Solid State Commun. **74**, 613 (1990); Phys. Rev. B **43**, 1993 (1991); **43**, 8861 (1991).
[23] D. R. Hamann, M. Schlüter, and C. Chiang, Phys. Rev. Lett. **43**, 1494 (1979); M. T. Yin and M. L. Cohen, Phys. Rev. B **26**, 5668 (1982).
[24] J. P. Perdew and A. Zunger, Phys. Rev. B **23**, 5048 (1981).
[25] S. Ismail-Beigi and S. G. Louie, Phys. Rev. Lett. **95**, 156401 (2005).
[26] T. Uchino, M. Takahashi, and T. Yoko, Phys. Rev. Lett. **84**, 1475 (2000).
[27] K. Raghavachari, D. Ricci, and G. Pacchioni, J. Chem. Phys. **116**, 825 (2002).
[28] J. Sarnthein, A. Pasquarello, and R. Car, Phys. Rev. Lett. **74**, 4682 (1995).
[29] M.-Z. Huang and W. Y. Ching, Phys. Rev. B **54**, 5299 (1996).
[30] R. B. Laughlin, J. D. Joannopoulos, and D. J. Chadi, Phys. Rev. B **20**, 5228 (1979).
[31] A. Appleton, T. Chiranjivi, and M. Jafaripour, in *The Physics of SiO_2 and Its Interfaces*, edited by S. T. Pantelides (Pergamon Press, New York, 1978).
[32] S. T. Pantelides and W. A. Harrison, Phys. Rev. B **13**, 2667 (1976).
[33] A. Pasquarello and R. Car, Phys. Rev. Lett. **80**, 5145 (1998).
[34] A. E. Geissberger and F. L. Galeener, Phys. Rev. B **28**, 3266 (1983).

[35] H. Hosono, M. Mizuguchi, H. Kawazoe, and T. Ogawa, Appl. Phys. Lett. **74**, 2755 (1999).
[36] G. Pacchioni and G. Ieranó, Phys. Rev. Lett. **79**, 753 (1997).
[37] B. B. Stefanov and K. Raghavachari, Phys. Rev. B **56**, 5035 (1997).
[38] N. Capron *et al.*, J. Chem. Phys. **112**, 9543 (2000).
[39] G. Pacchioni and A. Basile, J. Non-Cryst. Solids **254**, 17 (1999).
[40] T. Uchino, M. Takahashi, and T. Yoko, Phys. Rev. Lett. **86**, 1777 (2001).
[41] S. Mukhopadhyay, P. V. Sushko, A. M. Stoneham, and A. L. Shluger, Phys. Rev. B **71**, 235204 (2005).
[42] D. Donadio, M. Bernasconi, and M. Boero, Phys. Rev. Lett. **87**, 195504 (2001).
[43] M. Boero, A. Pasquarello, J. Sarnthein, and R. Car, Phys. Rev. Lett. **78**, 887 (1997).
[44] P. E. Blöchl, Phys. Rev. B **62**, 6158 (2000).
[45] Z.-Y. Lu, C. J. Nicklaw, D. M. Fleetwood, R. D. Schrimpf, and S. T. Pantelides, Phys. Rev. Lett. **89**, 285505 (2002).
[46] G. Pacchioni and G. Ieranó, Phys. Rev. B **57**, 818 (1998).